International Journal of Biological Macromolecules 325 (2025) 147259

Contents lists available at ScienceDirect

International Journal of Biological Macromolecules

journal homepage: www.elsevier.com/locate/ijbiomac

Immobilization and SPR-based binding characterization of L-asparaginase on metal-chelated polymeric nanoparticles

Kübra Kaya [a], Samir Abbas Ali Noma [a], Monireh Bakhshpour-Yücel [a], Bilgen Osman [a,*]

[a] Bursa Uludag University, Faculty of Arts and Science, Department of Chemistry, 16059 Gorukle, Bursa, Turkey

ARTICLE INFO

Keywords:
L-asparaginase
IMAC nanoparticles
Enzyme immobilization
Biocatalyst stability
Protease resistance
Therapeutic enzyme delivery

ABSTRACT

In this study, poly(2-hydroxyethyl methacrylate–N-methacryloyl-(L)-histidine methyl ester–Cu^{2+}) [PHM—Cu^{2+}] nanoparticles were synthesized by emulsion polymerization and used as carriers for L-asparaginase (L-ASNase) immobilization. The nanoparticles were characterized using SEM-EDX, TEM, FTIR, Zeta potential analyses. The binding affinity of L-ASNase on metal-chelated polymeric nanoparticles was investigated *via* surface plasmon resonance (SPR) analysis. The immobilized enzyme (PHM-Cu^{2+}-L-ASNase) achieved an immobilization yield of 86.4 %, activity yield of 73.6 %, and immobilization efficiency of 85.1 %. The optimum pH shifted from 8.5 (free) to 7.0 (immobilized), and the optimum temperature from 45 °C to 50 °C. The PHM-Cu^{2+}-L-ASNase presented enhanced resistance to proteolysis. Kinetic studies revealed that K_m and V_{max} values decreased after immobilization, indicating increased substrate affinity. Immobilization also resulted in a slightly lower turnover number (k_{cat}) compared to the free enzyme. The PHM-Cu^{2+}-L-ASNase preserved 60 % activity after ten reuse cycles and maintained higher activity in the presence of various metal ions and organic solvents. Thermal, storage, and *in vitro* artificial human serum stability studies revealed that the PHM-Cu^{2+}-L-ASNase exhibited slower inactivation and extended half-life compared to the free L-ASNase. SPR analysis demonstrated high binding affinity (K_D = 0.016 IU/mL), fitting the Langmuir model. Consequently, the PHM—Cu^{2+} nanoparticles were effective carriers for L-ASNase enzyme, enhancing its catalytic activity, stability, and reusability for pharmaceutical and industrial use.

1. Introduction

Enzymes are biomolecules that act as catalysts in living organisms and regulate the rate of chemical reactions without undergoing any change during the process. Enzymes are immobilized to overcome the disadvantages associated with their free form and to significantly improve their activity, stability, and reusability [1]. Moreover, immobilized enzymes can be used in various reaction environments and under harsh conditions compared to free enzymes. The use of nanomaterials as solid support materials in enzyme immobilization is increasing day by day. Nanoparticles with a high surface area have a wide range of applications and offer significant advantages in the fields where they are utilized [2]. Nanoparticles are highly useful in applications based on surface interactions such as enzyme immobilization, controlled drug release, adsorption [3], purification, and surface modification. Reducing the size of nanoparticles increases their surface-to-volume ratio. The main production methods used to prepare polymeric nanoparticles include suspension, emulsion, bulk, core-shell, and solution polymerization. The choice of polymerization method depends on the solubility of the active substance and the structure of the polymer used.

L-Asparaginase (L-ASNase) is an important chemotherapeutic agent, particularly used in the treatment of acute lymphoblastic leukemia (ALL). The therapeutic effect of this enzyme arises from a structural vulnerability in leukemic cells: unlike normal cells, leukemic cells lack the enzyme asparagine synthetase and are therefore unable to synthesize the amino acid L-asparagine, which is essential for their survival [4]. L-ASNase degrades L-asparagine present in the extracellular environment, depriving leukemic cells of this critical amino acid and ultimately leading to their death [5]. Beyond its medical applications, L-ASNase has also been used in the food industry to reduce the formation of acrylamide, a potentially carcinogenic compound that forms during the high-temperature processing of starchy foods through the Maillard reaction [6,7]. Due to its ability to convert L-asparagine to L-aspartic acid, L-ASNase can be applied as a pretreatment without altering the taste or

* Corresponding author.
E-mail addresses: kbrakya44@gmail.com (K. Kaya), samir.abaas90@gmail.com (S.A.A. Noma), myucel@uludag.edu.tr (M. Bakhshpour-Yücel), bilgeno@uludag.edu.tr (B. Osman).

https://doi.org/10.1016/j.ijbiomac.2025.147259
Received 18 April 2025; Received in revised form 26 August 2025; Accepted 29 August 2025
Available online 30 August 2025
0141-8130/© 2025 Elsevier B.V. All rights are reserved, including those for text and data mining, AI training, and similar technologies.

texture of foods [8]. However, it is not always possible to eliminate acrylamide completely, as some contributing factors are independent of L-asparagine [9]. Because of its potential carcinogenicity, minimizing acrylamide in food is of great importance [10]. The enzyme has been applied to various products such as potatoes, French fries, bread, coffee, and biscuits, where reductions in acrylamide content of up to 99 % have been reported [7,11–14]. Currently, food-grade L-ASNase is commonly produced from *Aspergillus oryzae* and *Aspergillus niger* [15], and it has also been employed in biosensor systems to detect L-asparagine in food products [16]. Currently, the L-ASNase enzyme used in clinical applications is derived from bacterial sources. However, these bacterial enzymes can cause side effects such as fever, anaphylaxis, and hypersensitivity reactions [17]. In addition, their purification processes are costly and their availability for industrial-scale applications is limited [18]. As a result, the immobilization of the L-ASNase enzyme is gaining increasing importance. Immobilization aims to reduce the enzyme's side effects and prolong its half-life. However, the main challenge associated with this process is the loss of catalytic activity following immobilization. Therefore, there is a growing need to develop novel carrier systems capable of addressing this issue while preserving the enzyme's activity.

L-ASNase is a critical therapeutic enzyme used especially in the treatment of ALL and therefore, numerous immobilization strategies have been investigated to enhance its stability, activity, and reusability. Various supports such as levan [19], polyaniline nanofibers [20], poly (2-hydroxyethyl methacrylate) (pHEMA)-starch [21], and poly(methacrylic acid-co-methyl methacrylate) [P(MAA-co-MMA)]-starch composites [22] have shown improved enzyme stability and substrate affinity. Calcium alginate beads were optimized for encapsulation using response surface methodology [23], while graphene oxide modified with aspartic acid provided efficient covalent immobilization [24]. Nanostructures such as oxidized carbon nanotubes [25], magnetic poly (2-hydroxyethyl methacrylate-*co*-glycidyl methacrylate) [poly(HEMA-GMA)] nanoparticles [26], and functionalized Fe_3O_4/SiO_2 particles [27] enhanced thermal and storage stability. Cryogel-based supports further improved activity under harsh conditions [28]. Innovative carriers like Fe_3O_4@*Au*-carboxymethyl cellulose (CMC) nanoparticles [29], carbon xerogels [30], poly(amidoamine) (PAMAM) dendrimer-ZnO-chitosan hybrids [31], and smart nanopolymers [32] also demonstrated excellent catalytic efficiency and biocompatibility. These reports have highlighted the potential of advanced materials for the effective immobilization of L-ASNase in biomedical and industrial applications. Although numerous studies have been reported on the purification, immobilization, and sensor-based applications of L-ASNase, research focusing on its immobilization and application on biocompatible polymeric support materials for clinical purposes remains limited. Support materials used to enhance the stability and sensitivity of the enzyme include chitosan–tripolyphosphate nanoparticles [33], poly(methyl methacrylate-*co*-methacrylic acid)/starch composites [34], and pHEMA as well as pHEMA/starch composites [35].

In this study, poly(2-hydroxyethyl methacrylate–N-methacryloyl-(L)-histidine methyl ester– Cu^{2+}) [PHM—Cu^{2+}] nanoparticles were synthesized *via* emulsion polymerization [36] and used as support material for the immobilization of L-ASNase. The main objective was to employ metal-chelated polymeric nanoparticles for the efficient immobilization of L-ASNase, aiming to improve its stability, catalytic activity, and reusability, thereby enhancing its potential for pharmaceutical and biotechnological applications. The molecular-level binding affinity was evaluated using surface plasmon resonance (SPR) analysis. HEMA, widely used in biomedical applications due to its hydrophilic and biocompatible nature, and N-methacryloyl-(L)-histidine methyl ester (MAH), a histidine-derived monomer capable of forming strong interactions with protein-based enzymes, were used in the copolymer structure. Cu^{2+} ions were incorporated to promote high-affinity binding through metal-chelate interactions with amino acid residues on L-ASNase [37–39]. The PHM—Cu^{2+} and L-ASNase-immobilized PHM—Cu^{2+} (PHM-Cu^{2+}-L-ASNase) nanoparticles were characterized using scanning electron microscopy with energy-dispersive X-ray spectroscopy (SEM-EDX), Fourier transform infrared (FTIR) spectroscopy, transmission electron microscopy (TEM) and zeta potential analysis. The activity of free and immobilized L-ASNase was evaluated under various conditions including pH, temperature, thermal and storage stability, protease resistance, reusability, the presence of metal ions, and organic solvents. In addition, enzyme activity was tested in artificial human serum. This study was the first to employ the PHM—Cu^{2+} matrix for the immobilization of a therapeutic enzyme with clinical relevance. By integrating SPR-based binding affinity analysis and multi-model kinetic evaluations, the study provided a comprehensive assessment L-ASNase stability and biocompatibility under pharmaceutically and physiologically relevant conditions.

2. Materials and methods

2.1. Materials

Sterile white freeze-dried powdered L-ASNase was purchased from ProSpec. L-asparagine, aluminum chloride, ammonium persulfate, ethylene glycol, ethylene glycol dimethylacrylate (EGDMA), sodium bicarbonat, sodium bisulfite, sodium hydroxide and trichloroacetic acid were purchased from Sigma (St. Louis, USA). L-Histidine methyl ester dihydrochloride and polyvinyl alcohol (PVA) were purchased from Aldrich (Munich, Germany). Copper (II) nitrate trihydrate and tris (hydroxy)-aminomethane were products of Merck (Darmstadt, Germany). Trypsin from porcine pancreas was purchased from Sigma-Aldrich. Potassium chloride, magnesium chloride hexahydrate, and calcium chloride were obtained from Merck. Lithium chloride, cobalt(II) chloride hexahydrate, cadmium chloride monohydrate, and aluminum chloride were purchased from Sigma-Aldrich. The water used in the experiments was purified using an Elga Flex3 ultrapure water device (Veloia Water Solutions & Technologies, France).

2.2. Synthesis of the MAH monomer

For the synthesis of MAH monomer; 5.0 g L-histidine methyl ester was dissolved in 100 mL dichloromethane (DCM). The solution was cooled to 0 °C, triethylamine and methacryloyl chloride were slowly added and stirred for 2 h. Then it was removed from the ice bath and kept in the stirrer for 24 h. The resulting MAH monomer was extracted with 10 % NaOH. After removal of DCM by rotary evaporator, the monomer was dissolved in ethyl alcohol [40].

2.3. Synthesis of the PHM—Cu^{2+} nanoparticles

The PHM—Cu^{2+} nanoparticles were synthesized by emulsion polymerization. EGDMA was used as the crosslinker, HEMA and MAH as the comonomer and monomer, respectively. Firstly, 1.0 mmol of the MAH monomer was mixed with 1.0 mmol of Cu^{2+} ion ($Cu(NO_3)_2.3H_2O$) to prepare MAH-Cu^{2+} complex. The prepared solution was stirred for 1 h at room temperature. For the preparation of the polymerization mixture, three separate solutions were prepared as phase I, phase II and organic phase (oil phase). For phase I, PVA, sodium dodecyl sulphate (SDS) and $NaHCO_3$ were dissolved in 5 mL of ultrapure water. For phase II, PVA and SDS were dissolved in 100 mL ultrapure water. The final phase III, also called organic phase, was prepared by mixing HEMA and EGDMA. The MAH-Cu^{2+} complex, which was previously prepared at a ratio of 1:1 (mmol/mmol), and phase I were added to the organic phase and mixed in a homogeniser (IKA-T 25 digital Ultra-Turrax®) at 20,000 rpm for 20 min. Then, the mixture was transferred to phase II in a glass flask. After the addition of sodium bisulfite and ammonium persulfate (APS) initiator pair to the reaction medium, the mixture was polymerised at a constant speed of 300 rpm and a constant temperature of 40 °C for 8 h. After the synthesis, the PHM—Cu^{2+} nanoparticles were centrifuged at

8000 rpm and washed with ethanol and water at 15,000 rpm for 30 min until the unreacted monomers and surfactants were removed. The obtained PHM—Cu^{2+} nanoparticles were then dried in a vacuum oven (Binder) at 40 °C. The nanoparticles were stored at 4 °C until use.

2.4. Characterization of the PHM—Cu^{2+} nanoparticles

The morphological characteristics of the PHM—Cu^{2+} nanoparticles were examined by SEM, while the presence of Cu^{2+} ions was confirmed through EDX analysis using a Carl Zeiss Gemini 300 SEM-EDX instrument. The PHM—Cu^{2+} nanoparticles were further visualized using high contrast transmission electron microscopy (CTEM) (FEI Tecnai G2 Spirit Biotwin, Hillsboro, USA). For CTEM analysis, the nanoparticles were dispersed in ethanol and incubated in a water bath until a homogeneous suspension was obtained. Then, a 10 μL aliquot of the suspension was dropped onto a carbon-coated copper grid and allowed to dry completely. Bright-field imaging mode was used to capture the images of the PHM—Cu^{2+} nanoparticles. The Zeta potential of the PHM—Cu^{2+} nanoparticles was determined using a Zeta potential analyzer (Malvern Instruments, UK).

2.5. Immobilization of L-ASNase

100 mg of the PHM—Cu^{2+} nanoparticles were mixed with the L-ASNase enzyme solution (100 U, pH 7.0) for immobilization of L-ASNase onto the nanoparticles. The mixture was incubated at 4 °C for 24 h. Then PHM-Cu^{2+}-L-ASNase nanoparticles were centrifuged at 8000 rpm at 4 °C. Then, the nanoparticles were washed 2 times with purified water to remove non-specifically bound enzyme. The nanoparticles were dried at room temperature and stored at 4 °C for further analysis. After that, the immobilization yield (I.Y), activity yield (A.Y) and immobilization effectiveness (I.E) were calculated using the following equations: Eqs. (1), (2) and (3), respectively.

$$\textit{Immobilization yield}\ (\%) = \frac{C_i - C_s}{C_i} \times 100 \tag{1}$$

$$\textit{Activity yield}\ (\%) = \frac{A_i}{A_f} \times 100 \tag{2}$$

$$\textit{Immobilization}\ \text{effectiveness}\ (\%) = \frac{\textit{Activity yield}}{\textit{Immobilization yield}} * 100 \tag{3}$$

In Eq. (1), C_i is the total protein concentration of the enzyme and C_s is the total protein concentration of unbound enzyme in the washing solutions and supernatant. In Eq. (2), A_i represents for the PHM-Cu^{2+}-L-ASNase activity and A_f represents for the free L-ASNase activity.

2.6. L-ASNase enzyme assay

For the determination of L-ASNase enzyme activity, the Nesslerization method developed by Mashburn in 1964 was used [41]. The method is based on the quantification of ammonia released from the hydrolysis of L-asparagine by L-ASNase. Accordingly, substrate solution (10 mM, 1 mL) and Tris-HCl buffer (50 mM, pH 8.6) were added to both free and immobilized L-ASNase preparations. The resulting mixtures were incubated at 50 °C for 15 min. The enzymatic reaction was then terminated by the addition of trichloroacetic acid (TCA) solution (1.5 M, 100 μL). Subsequently, 100 μL of the reaction mixture was transferred to the 96-well plates, followed by the addition of 100 μL of Nessler's reagent (potassium tetraiodomercurate, K_2HgI_4). After incubation at room temperature for 10 min, the absorbance of the yellow-orange colored solution was measured spectrophotometrically at 480 nm using an 800 TS microplate reader. Enzyme activity (IU) was defined as the amount of enzyme that releases 1 μmol of ammonia per minute under optimal conditions. All experiments were performed in triplicate. The results were expressed as relative activity (%), with the highest activity value taken as 100 %.

2.7. Effect of pH and temperature

To determine the optimum pH, free and immobilized enzymes were treated with substrate solutions prepared with various pH buffers at room temperature. Substrate solutions were prepared using citrate (pH 4.0, 5.0, 6.0), phosphate (pH 7.0, 7.5, 8.0) and Tris-HCl (pH 8.5, 9.0, 10.0) buffers. Furthermore, the activities of free and immobilized enzymes were measured separately using standard assay conditions at temperatures ranging from 30 to 60 °C in 5 °C intervals. The optimum pH and temperature values were considered 100 % for residual activity calculation.

2.8. Thermal and storage stability

To evaluate the thermal stability of free L-ASNase and PHM-Cu^{2+}-L-ASNase, they were incubated at 50 °C for 3 h at various times (0, 15, 30, 45, 60, 90, 120, 150, 180 min). At the end of each dwell time, the standard enzyme activity measurement was performed to determine the remaining enzyme activity. The activity value recorded at 0 min was considered as control. The storage stability of free and immobilized enzymes was investigated by keeping both enzyme samples at room temperature for 4 weeks. The enzyme activity measured on the first day was accepted as 100 % and other activities were compared with the initial activities.

The thermal and storage stability profiles of free L-ASNase and PHM-Cu^{2+}-L-ASNase were evaluated by fitting the experimental data to three commonly used kinetic inactivation models: first-order, biphasic, and Weibull distribution models. All fittings and regression analyses were performed using MATLAB program. Half-life values ($t_{1/2}$) were calculated from the fitted parameters according to each model's definition.

2.9. Proteolytic resistance

The low stability of bacterial enzymes used as medicinal drugs against proteases can cause major problems. Therefore, 100 U of the free L-ASNase and PHM-Cu^{2+}-L-ASNase were incubated with 100 μL trypsin solution (0.5 mg/mL) (0 min–120 min) to determine the resistance of both free and immobilized L-ASNase enzyme against trypsin enzyme. The enzyme activity was measured by adding 1 mL of substrate solution (10 mM) to the sample taken at the specified times.

2.10. Kinetic parameters

The kinetic parameters (*Km* and *Vmax*) of free L-ASNase and PHM-Cu^{2+}-L-ASNase enzymes were determined. For this purpose, the substrate solutions at different concentrations (0.25, 0.50, 0.75, 1, 2, 3, 4, 6 and 8 mM) were prepared, and initial reaction rates were measured under optimal conditions (50 °C, pH 8.0) using the standard enzyme activity assay. *Km* and *Vmax* values were calculated using the Lineweaver-Burk equation (Eq. (4)).

$$\frac{1}{V_0} = \frac{K_m}{V_{max}} \frac{1}{[S]} + \frac{1}{V_{max}} \tag{4}$$

In Eq. (4), V_o represents the initial reaction rate, [S] denotes the concentration of the substrate (mM), *Vmax* is the maximum reaction rate (μmol/min), and *Km* refers to the Michaelis-Menten constant (mM). The kcat values for the free and immobilized enzymes were also calculated by dividing the Vmax values by the enzyme amount.

2.11. Reusability of the PHM-Cu^{2+}-L-ASNase

The reusability of PHM-Cu^{2+}-L-ASNase under optimum conditions was evaluated. After each measurement, the PHM-Cu^{2+}-L-ASNase nanoparticles were removed from the reaction medium and washed with

buffer, followed by addition of new substrate for the next reaction cycle. The activity of the supernatant was determined using the standard enzyme activity measurement. The first measured enzyme activity was considered to have 100 % relative activity and the process was repeated ten times.

2.12. Metal ions and solvent effect

To evaluate the effect of metal ions and organic solvents on the free L-ASNase and PHM-Cu^{2+}-L-ASNase activities, both enzymes were incubated in 1 mL of 10 mM different metal ion (K^+, Li^+, Ca^{2+}, Cd^{2+}, Co^{2+}, Mg^{2+}, Al^{3+}) solutions for 24 h at room temperature and their activities were measured under optimum conditions (50 °C, pH 8.0). The following metal salts were used for the experiments: KCl, $MgCl_2{\cdot}6H_2O$, $CaCl_2$, LiCl, $CoCl_2{\cdot}6H_2O$, $CdCl_2{\cdot}H_2O$, $AlCl_3$. To investigate the effect of organic solvents (acetone, acetonitrile, ethanol, ethyl acetate, ethylene glycol, DCM and dimethyl sulfoxide (DMSO)) on the activity of the free and immobilized enzymes, both enzymes were incubated with organic solvents (5 % *v*/v, 1 mL) at 25 °C for 24 h and their activities were measured. The activity of solutions free of organic solvents and metal ions was considered as 100 %.

2.13. Determination of in vitro half-life

The determination of *in vitro* half-life is crucial for assessing the potential applicability of the free and immobilized L-ASNase in various biological applications. For this purpose, the free L-ASNase and PHM-Cu^{2+}-L-ASNase (1000 U) were incubated with artificial serum at 37 °C for 1 week. The activity of free and immobilized enzymes was measured daily to calculate their *in vitro* half-lives. For this purpose, the initial day's activity for both free and immobilized enzymes was considered as 100 %. Changes in the enzyme activity were calculated as relative activity. The *in vitro* inactivation kinetics of the free and PHM-Cu^2-L-ASNase in artificial human serum were evaluated using first-order, Weibull distribution, and biphasic models.

The first-order model assumes that the rate of enzyme inactivation is directly proportional to the concentration of active enzyme remaining at any given time, resulting in a single-phase exponential decay and a constant rate of fractional activity loss over time. Eq. (5) was used to calculate first-order inactivation model parameters

$$A_t = A_o e^{-kt} \tag{5}$$

The Weibull distribution model assumes that the rate of enzyme inactivation is time-dependent and follows a flexible, non-linear pattern (Eq. (6)).The model does not presume distinct kinetic phases but rather models the overall decay profile continuously.

$$A_t = A_o e^{-kt^n} \tag{6}$$

The biphasic model assumes that enzyme inactivation occurs through two parallel and independent first-order processes, each with its own rate constant. It presumes the enzyme population consists of two fractions—one that deactivates rapidly and another more slowly—resulting in a double-exponential decay profile. The non-linear equation of the biphasic model was given in Eq. (7).

$$A_t = A_0\left[fe^{-k_1 t} + (1-f)e^{-k_2 t}\right] \tag{7}$$

In the applied kinetic models, k represents the inactivation rate constant (time^{-1}, time^{-n}), reflecting the speed at which enzymatic activity decreases over time. A_t represents the relative enzyme activity (%) at time t, while A_0 denotes the initial enzyme activity. The parameter f denotes the fraction of the enzyme population undergoing rapid (fast-phase) inactivation in biphasic models. The shape parameter n used in the Weibull distribution model indicates the time-dependence of the inactivation process; values of $n<1$ suggest a decelerating rate, $n=1$ implies constant-rate (first-order) behavior, and $n>1$ indicates an accelerating inactivation behavior.

2.14. SPR analysis of L-ASNase binding to the PHM—Cu^{2+} nanoparticles

The real-time binding interaction between the L-ASNase and the PHM—Cu^{2+} nanoparticles was investigated using SPR analysis. For this purpose, the PHM—Cu^{2+} nanoparticles were immobilized onto the gold surface of an SPR sensor chip. Prior to nanoparticle deposition, the gold surface was subjected to a modification process. The process began with cleaning the gold chips using an alkaline piranha solution (3:1, *v*/v, NH_4OH/H_2O_2). The chips were immersed in 10 mL of the cleaning solution for 5 min, then rinsed with ethanol and dried in a vacuum oven at 200 mmHg and 35 °C for 2 h. Subsequently, the gold chips were immersed in an ethanol/water solution (4:1, *v*/v) containing 3.0 mM allyl mercaptan and incubated for 24 h to enable the formation of a self-assembled monolayer. Then, the chips were rinsed with ethanol and dried using nitrogen gas. The PHM—Cu^{2+} nanoparticle suspension (0.5 mg/mL) was applied to the surface of the chips *via* droplet deposition, followed by drying in a vacuum oven at 200 mmHg and 35 °C.

SPR analysis was conducted using the SPR Imager II system (GWC Technologies, Madison, USA) to monitor the binding of L-ASNase in real time. Initially, the SPR sensor surface was rinsed with 50 mL of deionized water, after which an appropriate buffer solution was introduced for approximately 3 min to allow for equilibration. Following the equilibration phase, the L-ASNase solutions at various concentrations were introduced sequentially (5 mL each) at a flow rate of 150 μL/min. The resulting shift in resonance angle was continuously monitored. After equilibrium was reached, typically within approximately 10 min, a desorption step was initiated by introducing 10 mL of a 10 % ethylene glycol solution at the same flow rate. The sensorgram obtained typically displayed distinct association and dissociation phases, which are critical for determining the binding kinetics. After the desorption step, the SPR sensor surface was rinsed with deionized water and buffer solution. The adsorption–desorption–cleaning steps were repeated prior to the introduction of each new concentration of L-ASNase solution. To determine the optimal pH for L-ASNase binding, the enzyme solutions were prepared in phosphate buffers with different pH values, specifically pH 5.0, 6.0, 7.0, 7.4, and 8.0. The sensograms recorded by passing the L-ASNase solutions at a concentration of 1000 IU/mL at different pHs are given in the supporting information (Fig. SI1). The pH value that resulted in the highest binding response (pH: 7.0) was selected for all subsequent experiments. Binding studies were then continued using the L-ASNase solutions at concentrations ranging from 100 to 2000 UI/mL at pH 7.0.

3. Results and discussion

3.1. Properties of the PHM-Cu^{2+}-L-ASNase nanoparticles

Immobilized metal affinity chromatography (IMAC) is a technique based on the binding of proteins to the coordination sites of metal ions. The technique is mainly based on the interactions between a metal ion chelated with histidine on the surface of the protein and a ligand immobilized to the support material [37–47]. Commonly used metal ions in IMAC are Cu(II), Ni(II), Zn(II), Co(II), Ca(II) and Fe(III) ions [48–50]. The technique has been widely applied for the purification of histidine-tagged proteins, natural metal-binding proteins, and antibodies [51]. With the presence of Cu^{2+} ions in the PHM—Cu^{2+} polymeric structure, it was aimed that the nanoparticles show high affinity for L-ASNase protein. In our previous studies, PHM—Cu^{2+} nanoparticles gave successful results in the determination of breast cancer MDA MB 231 cell, ovarian cancer marker carbohydrate antigen-125, and pesticides [52–54]. The HEMA monomer used in the synthesis of PHM—Cu^{2+} nanoparticles has been widely used due to its superior properties such as hydrophilicity, low toxicity, and biocompatibility [55,56].

The structure, surface morphology, and approximate size of the PHM—Cu^{2+} polymeric nanoparticles were elucidated by SEM and TEM

analyses. SEM images of the nanosized PHM—Cu^{2+} and PHM-Cu^{2+}-L-ASNase nanoparticles obtained at different magnification ratios are shown in Fig. 1. The SEM images clearly indicated that the emulsion polymerization procedure enabled the synthesis of PHM—Cu^{2+} nanoparticles in approximately spherical form. The diameter of the PHM—Cu^{2+} nanoparticles was around 50 nm (Fig. 1b).The size of the nanoparticles provided a significant advantage for intracellular uptake in therapeutic applications. It has been known that smaller, spherical, and positively charged nanoparticles are internalized more efficiently *via* endocytosis and tend to remain in cells longer compared to larger, cylindrical, or negatively/neutral particles [57,58]. SEM images in Fig. 1c and Fig. 1d showed that the morphology of the PHM—Cu^{2+} nanoparticles did not change after L-ASNase immobilization. TEM images of the PHM—Cu^{2+} nanoparticles are given in Fig. 1d and e.

SEM-EDX analysis was also performed to determine the elemental composition of the PHM—Cu^{2+} and PHM-Cu^{2+}-L-ASNase nanoparticles (Fig. SI2). The analysis revealed the presence of carbon (C), nitrogen (N), oxygen (O) and copper (Cu) atoms in the PHM—Cu^{2+} and PHM-Cu^{2+}-L-ASNase nanoparticles. Moreover, the PHM-Cu^{2+}-L-ASNase nanoparticles contained sulfur (S) (0.66 %). After immobilization, nitrogen content increased from 1.10 % to 1.45 %, oxygen content increased from 5.59 % to 11.32 %, carbon content decreased from 92.28 % to 86.51 % and copper content decreased from 1.03 % to 0.06 %. The decrease in copper content may be attributed to the surface masking effect of the enzyme layer. Additionally, coordination of the enzyme to Cu^{2+} may cause local redistribution, suggesting possible interaction between Cu^{2+} ions and L-ASNase. As a result, the elemental composition of PHM—Cu^{2+} nanoparticles changed after immobilization. The presence of S atom in the structure of PHM—Cu^{2+} nanoparticles proved that the L-ASNase enzyme was successfully immobilized.

FTIR analysis of the nanoparticles was performed in the range of 4000–400 cm^{-1} to characterize the chemical structure. The FTIR spectra are shown in Fig. SI3. In the FTIR spectrum of free L-ASNase, the O—H stretching band was located at 3283 cm^{-1}, and the alkyl group (-CH_2) appeared at 2963 cm^{-1}. The characteristic bands at 1638 cm^{-1}, 1535 cm^{-1}, and 1450 cm^{-1} corresponded to the amide I, amide II, and amide III bands, respectively. The absorption bands at 1236 cm^{-1} and 1158 cm^{-1} corresponded to aliphatic amines (C—N bond stretching). In the spectrum of PHM—Cu^{2+} nanoparticles, absorption bands for repeating aliphatic C—H bonds were observed at 2956 cm^{-1}, and a band for the ester carbonyl (C=O) group was found at 1725 cm^{-1}. The presence of amide bonds in the spectrum indicated that metal chelating monomers were included in the structure of PHM—Cu^{2+} nanoparticles [40]. Similar to the free L-ASNase spectrum, the nanoparticles exhibited C—N stretching bands at 1255 cm^{-1} and 1149 cm^{-1}. The absorption band detected at 3454 cm^{-1} was attributed to the N—H stretching band from the monomer [59]. Additionally, the characteristic peaks observed in the range of 500–400 cm^{-1} corresponded to Cu—N stretching bands. In the spectrum of PHM-Cu^{2+}-L-ASNase nanoparticles, the characteristic amide bands were observed. The ester carbonyl group was observed at 1725 cm^{-1}, and aliphatic C—H bonds appeared at 2990 cm^{-1} and 2951 cm^{-1}. Furthermore, the peaks observed at 1258 cm^{-1} and 1152 cm^{-1} corresponded to C—N vibrations.

Zeta potential is used in colloid chemistry to observe the behavior of dispersive systems in liquids. Nanoparticles with a Zeta potential between −10 and +10 mV are considered neutral. In addition, nanoparticles with Zeta potential greater than +30 mV are considered strong cationic and nanoparticles with Zeta potential less than −30 mV are considered strong anionic [60]. The results showed that the Zeta potential value of PHM—Cu^{2+} nanoparticles was −20.1 mV. It is generally accepted in the literature that a Zeta potential of more than +25 mV or less than −25 mV provides sufficient repulsive force to prevent particle aggregation [61–64]. The PHM-Cu^{2+}-L-ASNase nanoparticles had very high stability and tended to aggregate to a certain degree in aqueous solution. However, there were no practical difficulties during immobilization and use.

3.2. Immobilization efficiency

The immobilization parameters were evaluated in terms of I.Y, I.E and A.Y. The I.Y was calculated as 86.4 ± 3.3 %, the A.Y. 73.6 ± 4.7 % and the *I.E.* 85.1 ± 4.3 %. It can be stated that the obtained values were high, demonstrating that the support binded to L-ASNase with high affinity and without a significant change in its native conformation. When compared to the existing reports, the obtained values were considerably favorable. For example, Bahraman and Alemzadeh reported an I·Y of 34.49 % for *E. coli*-derived L-ASNase encapsulated in calcium alginate beads [23]. Monajati et al. achieved 100 % immobilization and activity recovery on graphene oxide modified with L-aspartic acid, representing one of the few cases with complete retention [24]. Haroun et al. observed a moderate I.Y of 54.4 % yet maintained 100 % activity recovery using oxidized multi-walled carbon nanotubes [25]. In a cryogel-based system, Noma et al. reported an I.Y of 68.8 % and an A.Y of 69.3 % [28]. Tarhan et al. achieved 68 % I.Y using Fe_3O_4@Au-CMC magnetic nanoparticles [29], while Barros et al. recorded [30] both I.Y and A.Y at 100 % with carbon xerogels under optimized conditions. In contrast, Vina et al. [19] achieved 55 % A.Y without reporting I.Y, highlighting variability depending on the support material and method used. The high I.E obtained in this study (85.1 %) suggested that the support exhibited strong affinity toward L-ASNase. This is likely attributed to the chelation of Cu^{2+} ions within the PHM—Cu^{2+} nanoparticles, which may have enhanced the binding interaction.

3.3. Optimal pH and temperature

The effect of pH on the activities of free and immobilized enzymes was determined by measuring their activities at different pH values (4.0–10.0). While the optimum pH of free L-ASNase was 8.5, the optimum pH of immobilized L-ASNase was determined as 7.0 (Fig. 2a). The observed shift in the optimum pH can be attributed to interactions between the enzyme and the support matrix, which may have altered the local microenvironment around the enzyme's active site. In particular, the coordination of Cu^{2+} ions with basic functional groups (histidine imidazole) in the PHM structure may create a locally more alkaline environment near the enzyme. Consequently, the enzyme requires a lower bulk pH to maintain the optimal protonation state of catalytic residues, leading to maximum activity at a more acidic pH. Such changes have been frequently reported in the literature and were generally associated with modifications in the surface properties of the support or enzyme conformation. For instance, Ulu et al. [21] reported no shift in optimum pH (remaining at 8.5), whereas Ulu et al. [22] observed improved pH tolerance upon immobilization. However, in several other studies, a downward shift in pH optimum has been noted: Orhan and Uygun [26] reported a decrease from pH 7.5 to 6.5, and Tarhan et al. [29] found an optimum pH of 7.0 for immobilized L-ASNase, both indicating a drift toward acidic conditions. Baluchi and Homaei [65] reported an increase in optimum pH (from 8.0 to 9.0) after immobilization on chitosan nanoparticles. Our results revealed a shift toward a neutral region, which was advantageous for pharmaceutical applications. Moreover, the immobilized enzyme retained 75 % activity at pH 10, compared to 54 % for the free enzyme, demonstrating enhanced resilience in basic environments. Therefore, the ability of our immobilization strategy to enhance enzyme performance in basic media not only differentiated it from many existing approaches but also highlighted its potential for broader practical applications.

The shift in optimum temperature from 45 °C (free enzyme) to 50 °C (immobilized enzyme) observed in the present study reflected an enhancement in the thermal resistance of L-ASNase upon immobilization (Fig. 2b). The shift was consistent with trends reported in the literature, where immobilization generally contributed to improved enzyme rigidity and resistance to thermal denaturation. For example, Orhan and Uygun [26] reported a similar increase in optimum temperature from 45 °C to 55 °C after immobilizing L-ASNase on magnetic

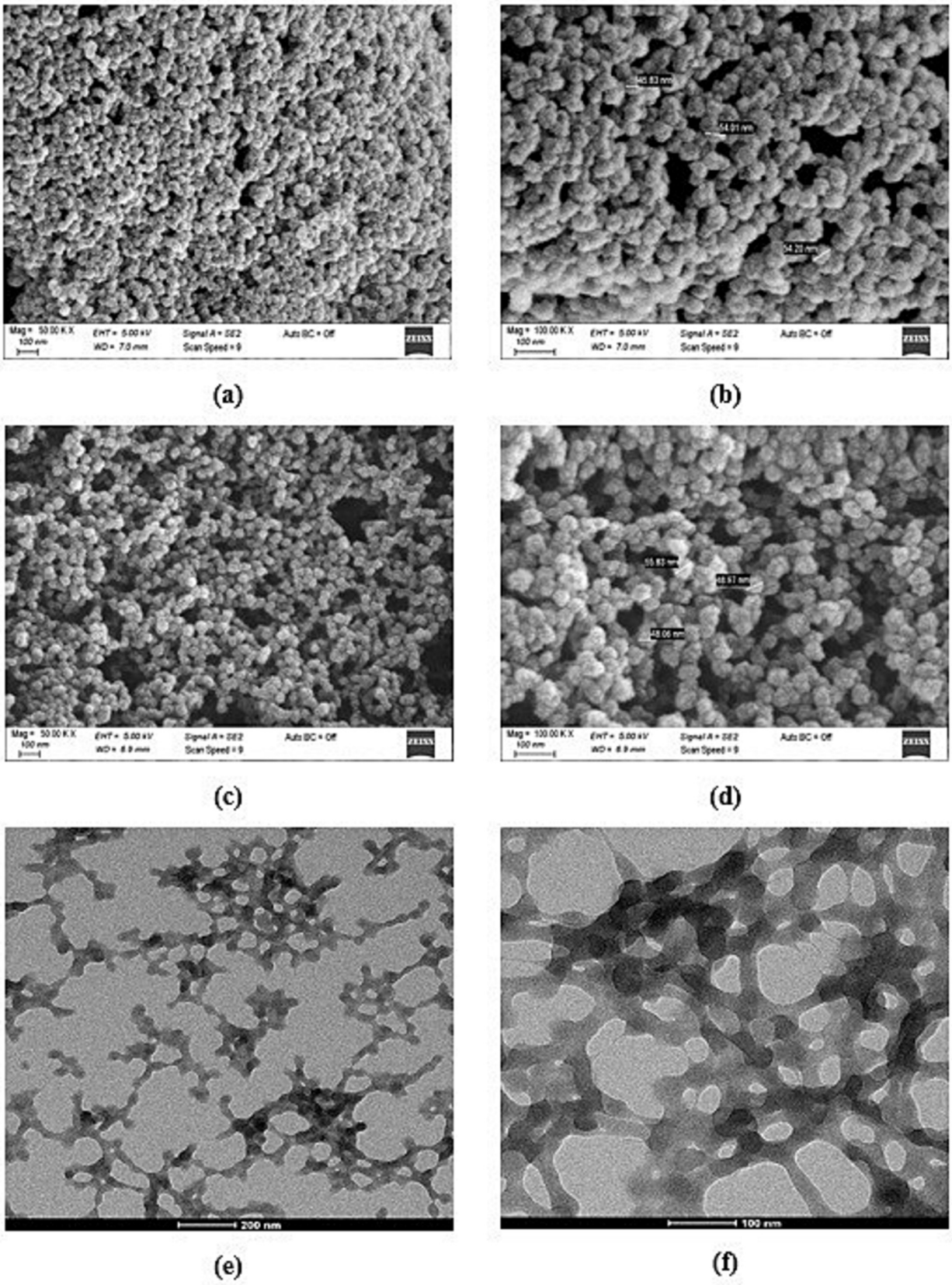

Fig. 1. SEM images of (a, b) the PHM—Cu^{2+} nanoparticles, (c, d) the PHM-Cu^{2+}-L-ASNase nanoparticles and (e, f) TEM images of the PHM—Cu^{2+} nanoparticles at different magnification ratios *Abbreviations*: PHM—Cu^{2+}, poly(2-hydroxyethyl methacrylate–N-methacryloyl-(L)-histidine methyl ester–Cu^{2+}); L-ASNase, L-asparaginase.

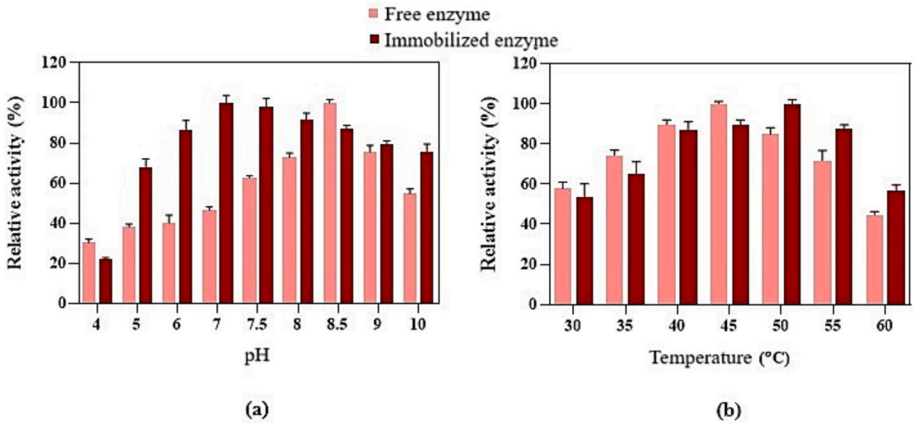

Fig. 2. (a) pH and (b) temperature effect on the free enzyme (L-ASNase) and immobilized enzyme (PHM-Cu^{2+}-L-ASNase) *Abbreviations*: L-ASNase, L-asparaginase; PHM—Cu^{2+}, poly(2-hydroxyethyl methacrylate–N-methacryloyl-(L)-histidine methyl ester–Cu^{2+}).

poly(HEMA-GMA) nanoparticles. Tarhan et al. [29] also observed an optimum temperature of 50 °C for immobilized enzyme, while the free enzyme displayed lower thermal tolerance. In contrast, some studies have reported no change in the optimum temperature but still demonstrated improved activity retention at elevated temperatures [21,22]. In our study, the PHM-Cu^{2+}-L-ASNase retained approximately 56 % of its activity at 60 °C, whereas the free enzyme retained only 44 %, highlighting a considerable improvement in high-temperature stability. Similar thermal stabilization was also reported by Baluchi and Homaei [65], who observed an increase in optimum temperature from 40 °C to 50 °C after immobilization on chitosan nanoparticles. As a result, the immobilized enzyme demonstrated a significant thermal stability while maintaining high catalytic activity. The ability to retain over half of the enzymatic activity at 60 °C suggested that the PHM-Cu^{2+}-L-ASNase nanoparticles could be a robust candidate for biotechnological processes requiring elevated operational temperatures.

3.4. Thermal and storage stability

The thermal stability of free L-ASNase and PHM-Cu^{2+}-L-ASNase was determined at 50 °C for specific times (0, 15, 30, 45, 45, 60, 90, 120, 150, 180 min) (Fig. 3a). The thermal stability profile of PHM-Cu^{2+}-L-ASNase demonstrated a substantial improvement over the free enzyme, particularly at 50 °C, where the immobilized enzyme retained approximately 60 % of its initial activity after 180 min, compared to only 34 % for the free form. The enhanced stability can be attributed to the coordination interactions between the enzyme and the support matrix, which likely restrict conformational mobility and prevent thermal denaturation. Similar improvements have been reported in the literature. For example, Barros et al. [30] observed that L-ASNase immobilized on carbon xerogels maintained 97 % of its initial activity after thermal exposure, while Orhan and Uygun [26] reported that immobilized L-ASNase preserved 50 % activity after 10 h at elevated temperatures, whereas the free enzyme was almost completely inactivated. In another study, Noma et al. [28] showed that cryogel-immobilized enzyme maintained 52 % of its activity after 10 reuse cycles and displayed improved thermodynamic parameters, including lower activation energy. Compared to these findings, the PHM-Cu^{2+}-L-ASNase developed in the current study offered comparable or superior stability, indicating that the structural rigidity conferred by the support matrix effectively mitigated the enzyme inactivation under thermal stress.

In order to better understand the thermal inactivation behavior of free L-ASNase and PHM-Cu^{2+}-L-ASNase, the first-order [66], biphasic [67,68], and Weibull distribution [69] models were applied to the experimental data obtained over a 180-min period at 50 °C. The fitted kinetic parameters and corresponding half-life values ($t_{1/2}$) for thermal inactivation are summarized in Table 1.

The parameters shown in Table 1 demonstrated that the first-order and Weibull distribution models provided nearly identical fits (R^2adj = 0.9908 and 0.9896, respectively), with comparable inactivation rate constants and half-lives (~116 min) for the free L-ASNase. The Weibull shape parameter (n = 1.011) indicated a nearly ideal first-order behavior. In contrast, the PHM-Cu^{2+}-L-ASNase showed a better fit with the Weibull distribution model (R^2adj = 0.9269) compared to the

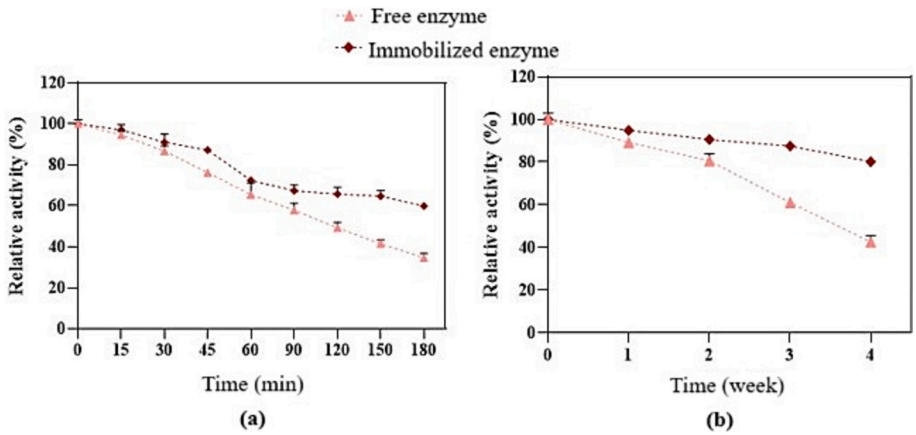

Fig. 3. (a)Thermal stability and (b) storage stability of the free enzyme (L-ASNase) and immobilized enzyme (PHM-Cu^{2+}-L-ASNase) *Abbreviations*: L-ASNase, L-asparaginase; PHM—Cu^{2+}, poly(2-hydroxyethyl methacrylate–N-methacryloyl-(L)-histidine methyl ester–Cu^{2+}).

Table 1
Thermal inactivation kinetic parameters of the free enzyme (L-ASNase) and immobilized enzyme (PHM-Cu^{2+}-L-ASNase).

Parameter/ Model	First-order	Biphasic	Weibull distribution
Free L-ASNase			
k (min^{-1})	0.00595	$k_1 = 0.00704$; $k_2 = 0.00404$	0.00590
$t_{1/2}$ (min)	116.3	($t_{1/2}$ fast): 98.4; ($t_{1/2}$ slow): 171.5	116.02
R^2	0.9908	0.9909	0.9909
R^2adj	0.9908	0.9879	0.9896
RMSE	0.0224	0.0258	0.0239
SSE	0.00408	0.00400	0.00402
Parameters		f = 0.6811	n = 1.011
PHM-Cu^{2+}-L-ASNase			
k (min^{-1})	0.003347	$k_1 = 0.0125$;$k_2 = 0.001$	0.008597
$t_{1/2}$ (min)	207.8	($t_{1/2}$ fast): 55.43; ($t_{1/2}$ slow): 693.15	238.4
R^2	0.9040	0.9432	0.9269
R^2adj	0.9040	0.9351	0.9164
RMSE	0.0477	0.0392	0.0445
SSE	0.0182	0.0108	0.0139
Parameters		f = 0.3353	n = 0.802

Abbreviations: L-ASNase, L-asparaginase; PHM—Cu^{2+}, poly(2-hydroxyethyl methacrylate–N-methacryloyl-(L)-histidine methyl ester–Cu^{2+}); k, inactivation constant; $t_{1/2}$, half-life; R^2, coefficient of determination; R^2adj, adjusted coefficient of determination; RMSE, root mean square error; SSE, sum of squared errors; f, fraction of rapidly inactivated enzyme; n, shape parameter.

first-order model (R^2adj = 0.9040), and the shape parameter ($n = 0.802$) reflected a decelerating inactivation, consistent with the stabilizing effect of immobilization. The biphasic model provided a strong fit for both enzyme forms (R^2adj = 0.9879 for free L-ASNase and 0.9351 for immobilized L-ASNase), revealing two-phase inactivation behavior. In the immobilized enzyme, a lower fast-phase fraction (f = 0.3353 *vs.* 0.6811 in free L-ASNase) and a substantially longer slow-phase half-life (693.2 min *vs.* 171.5 min in free L-ASNase) highlighted the enhanced stability conferred by the support matrix. However, due to the limited time range of the experimental data (0–180 min), the half-life values corresponding to the slow phase (k_2) was extrapolated by the model rather than directly observed and should be interpreted with caution. The increase in half-life following immobilization confirmed the stabilizing effect of the PHM—Cu^{2+} matrix.

Storage stability is a critical factor for the practical application of enzymes, as their catalytic activity often declines over time. In the present study, the PHM-Cu^{2+}-L-ASNase exhibited superior long-term storage stability compared to the free enzyme (Fig. 3b). After four weeks at room temperature, the immobilized enzyme retained approximately 80 % of its initial activity, while the free enzyme retained only about 42 %, indicating a significant enhancement in stability. The obtained results were in good agreement with previous studies. For instance, Ulu et al. [22] reported that their immobilized L-ASNase system retained 60 % activity after 30 days at 25 °C, while Orhan and Uygun [26] observed that immobilized enzyme retained 30 % of its initial activity after 40 days, whereas the free enzyme lost all activity. Similarly, Noma et al. [28] showed that cryogel-immobilized L-ASNase preserved 54 % of its activity after 28 days. Compared to these findings, the storage stability of PHM-Cu^{2+}-L-ASNase was among the highest reported, suggesting that the coordination bond between the enzyme and the support material provided effective protection against degradation during storage. The prolonged stability made the PHM-Cu^{2+}-L-ASNase nanoparticles particularly advantageous for applications requiring long-term enzyme use without the need for frequent replenishment or refrigeration.

To evaluate the storage inactivation of free L-ASNase and PHM-Cu^{2+}-L-ASNase at room temperature, the inactivation kinetic models were also applied over a 5-week period. The fitted kinetic parameters and corresponding half-life values ($t_{1/2}$) are summarized in Table 2.

The results showed that the first-order and biphasic models presented similar fits (R^2 = 0.9148), with identical rate constants (k = 0.167 $wk.^{-1}$) and half-lives (~4.15 weeks) for the free enzyme, indicating uniform single-phase inactivation. The Weibull distribution model, however, provided a superior fit (R^2adj = 0.9864, RMSE = 0.0267), with a shape parameter n = 1.766, suggesting an accelerating inactivation behavior. For the immobilized enzyme, all models yielded high R^2 values, with the Weibull distribution model performing best (R^2adj = 0.9758, RMSE = 0.0116), and $n = 1.118$ indicating a time-dependent increase in inactivation rate. Half-life was 11.69 weeks. Although the biphasic model yielded a high R^2 value for both enzyme forms (0.9148 for free L-ASNase and 0.9784 for immobilized L-ASNase), the estimated parameters exhibited extreme uncertainty and no meaningful phase separation ($k_1 \approx k_2$) was observed.

3.5. Proteolytic resistance and reusability of the PHM-Cu^{2+}-L-ASNase

The low resistance of enzymes against protease enzymes is one of the biggest obstacles to pharmaceutical applications. In this study, the resistance of both free L-ASNase and PHM-Cu^{2+}-L-ASNase against trypsin hydrolysis was determined in detail (Fig. 4a). Proteolytic degradation is one of the primary limitations for the pharmaceutical use of therapeutic enzymes such as L-ASNase, as they are susceptible to inactivation by proteases like trypsin [70,71]. PEGylation is one of the key strategies to enhance the therapeutic efficacy of enzyme-based drugs. By forming a steric shield, it protects the enzyme from proteolytic degradation, thereby improving its stability and prolonging its biological activity [72]. The PHM-Cu^{2+}-L-ASNase demonstrated significantly higher resistance to trypsin-mediated hydrolysis compared to the free enzyme. After 120 min of incubation with trypsin, the free L-ASNase was almost completely degraded, whereas the immobilized enzyme retained approximately 45 % of its initial activity. The protection can be attributed to the coordination-based immobilization, which may shield cleavage sites or induce conformational rigidity that limits protease access. Although many immobilization studies have reported improvements in thermal or pH stability, relatively few have evaluated proteolytic resistance in detail. Notably, Haroun et al. [25] observed a decrease

Table 2
Storage inactivation kinetic parameters of the free enzyme (L-ASNase) and immobilized enzyme (PHM-Cu^{2+}-L-ASNase).

Parameter/ Model	First-order	Biphasic	Weibull distribution
Free L-ASNase			
k (wk^{-1})	0.167	$k_1 = k_2 = 0.167$	0.0719
$t_{1/2}$ (wk)	4.15	($t_{1/2}$ fast): 4.13; ($t_{1/2}$ slow): 4.16	3.61 wk
R^2	0.9148	0.9148	0.9898
R^2adj	0.9148	0.8296	0.9864
RMSE	0.0670	0.0947	0.0267
SSE	0.0179	0.0179	0.0021
Parameters		f = 0.4285	$n = 1.766$
PHM-Cu^{2+}-L-ASNase			
k (wk^{-1})	0.0507	$k_1 = k_2 = 0.0507$	0.0443
$t_{1/2}$ (wk)	13.66	($t_{1/2}$ fast): 13.66; ($t_{1/2}$ slow): 13.67	11.69
R^2	0.9784	0.9784	0.9819
R^2adj	0.9784	0.9569	0.9758
RMSE	0.0110	0.0155	0.0116
SSE	$4.820.10^{-4}$	$4.820.10^{-4}$	$4.050.10^{-4}$
Parameters		f = 0.3993	n = 1.118

Abbreviations: L-ASNase, L-asparaginase; PHM—Cu^{2+}, poly(2-hydroxyethyl methacrylate–N-methacryloyl-(L)-histidine methyl ester–Cu^{2+}); k, inactivation constant; $t_{1/2}$, half-life; R^2, coefficient of determination; R^2adj, adjusted coefficient of determination; RMSE, root mean square error; SSE, sum of squared errors; f, fraction of rapidly inactivated enzyme; n, shape parameter.

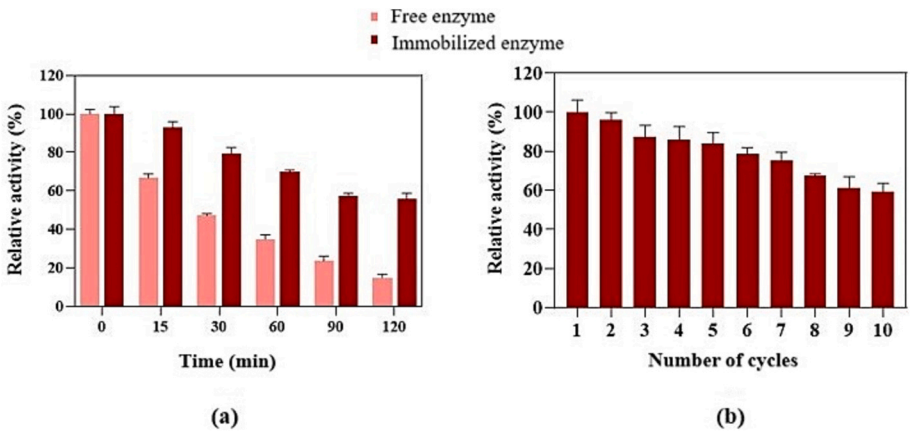

Fig. 4. (a) Protease resistance of the free enzyme (L-ASNase) and immobilized enzyme (PHM-Cu^{2+}-L-ASNase) and (b) the reusability of immobilized enzyme (PHM-Cu^{2+}-L-ASNase) *Abbreviations*: L-ASNase, L-asparaginase; PHM—Cu^{2+}, poly(2-hydroxyethyl methacrylate–N-methacryloyl-(L)-histidine methyl ester–Cu^{2+}).

in cytotoxicity and improved protease resistance after immobilizing L-ASNase onto oxidized carbon nanotubes, while Iraninasab et al. [31] demonstrated sustained enzyme release from a dendrimeric nanocarrier, indirectly suggesting resistance to proteolytic inactivation. As a result, the present study showed direct evidence of protease protection and underscores the potential of the PHM—Cu^{2+} immobilization matrix for therapeutic applications where enzymatic degradation by host proteases was a major concern.

Reusability is a key parameter for evaluating the economic feasibility of immobilized enzymes, particularly for industrial applications where repeated use is essential. In the present study, the immobilized L-ASNase retained approximately 60 % of its initial activity after multiple reaction cycles, demonstrating acceptable operational stability (Fig. 4b). Although a gradual decline in activity was observed, this may be attributed to potential structural alterations in the enzyme or partial enzyme leaching from the support material. Nonetheless, the retention of more than half of the initial activity indicated that the PHM-Cu^{2+}-L-ASNase nanoparticles were suitable for repeated use. Comparable results have been reported in the literature; for example, Barros et al. [30] observed 71 % activity retention after 6 cycles, while Tarhan et al. [29] reported that immobilized L-ASNase preserved over 75 % of its activity after 10 cycles. In another study, Noma et al. [28] noted that cryogel-immobilized enzyme retained 52 % activity after ten reuse cycles at room temperature. Although the PHM-Cu^{2+}-L-ASNase did not reach the highest levels of recyclability reported, it still demonstrated consistent and reliable performance under repeated use conditions, positioning it as a promising candidate for applications requiring multiple reaction cycles without substantial activity loss.

3.6. Kinetic parameters

Kinetic parameters for free and immobilized L-ASNase were calculated by Lineweaver-Burk plot (Fig. SI4). In addition to the Lineweaver-Burk plots used for parameter determination, Michaelis-Menten curves are given to illustrate the saturation kinetics of the enzymes (Fig. SI5). Kinetic parameters provided critical insights into the catalytic behavior of enzymes before and after immobilization (Table 3). The Km value for PHM-Cu^{2+}-L-ASNase was reduced from 5.49 mM (free enzyme) to 3.98 mM, indicating an increased substrate affinity following immobilization. This enhancement suggested that the immobilized enzyme can achieve maximum catalytic efficiency at lower substrate concentrations. Conversely, the Vmax value showed a slight reduction, from 243.90 μmol/min (free enzyme) to 188.68 μmol/min (immobilized enzyme), which may be attributed to diffusional limitations or restricted molecular flexibility upon immobilization. The results were in agreement with earlier studies; for example, Acet [32] reported a Km decrease from

Table 3
Kinetic parameters for the free enzyme (L-ASNase) and immobilized enzyme (PHM-Cu^{2+}-L-ASNase).

Enzyme form	Km (mM)	Vmax (μmol/min)	kcat (s^{-1})	kcat/Km (s^{-1}·mM^{-1})
Free L-ASNase	5.49	243.90	12.534×10^3	2.283×10^3
PHM-Cu^{2+}-L-ASNase	3.98	188.68	9.659×10^3	2.425×10^3

Abbreviations: L-ASNase, L-asparaginase; PHM—Cu^{2+}, poly(2-hydroxyethyl methacrylate–N-methacryloyl-(L)-histidine methyl ester–Cu^{2+}); Km, Michaelis constant; Vmax, maximum velocity; kcat, turnover number; kcat/Km, catalytic efficiency.

6.595 mM to 1.902 mM and a Vmax decrease from 212.766 μmol/min to 49.02 μmol/min upon immobilization of L-ASNase onto smart nanopolymers. Similarly, Ulu et al. [22] and Monajati et al. [24] observed a decrease in Km values after immobilization, reflecting improved substrate binding affinity. In a study, the L-ASNase enzyme was immobilized on graphite carbon nitride (g-C_3N_4) nanosheets *via* Ni^{2+} ions using the IMAC method, and it was found that the *Km* and *Vmax* values of the immobilized enzyme decreased compared to the free enzyme [30]. Although a moderate decrease in Vmax is commonly observed due to steric hindrance or mass transfer resistance, the significant reduction in Km in our study confirmed that the immobilization method enhanced the enzyme's functional performance.

The PHM–Cu^{2+}–L-ASNase exhibited a lower Vmax and, accordingly, a lower kcat compared with the free L-ASNase, which can be attributed to potential mass-transfer limitations, conformational restrictions, and partial shielding of the active sites caused by immobilization. However, immobilization onto the PHM—Cu^{2+} matrix reduced the Km value, indicating an increase in apparent affinity for the substrate. The catalytic efficiency (kcat/Km) of the immobilized enzyme was slightly higher than that of the free form (2.425×10^3 for immobilized enzyme and 2.283×10^3 s^{-1}·mM^{-1} for free enzyme). Although Vmax and kcat decreased for the PHM–Cu^{2+}–L-ASNase, the improved affinity suggested that the immobilized enzyme remained highly applicable.

3.7. Metal ion and organic solvent effect

The stability of the enzymes in the presence of metal ions (K^+, Li^+, Ca^{2+}, Cd^{2+}, Co^{2+}, Mg^{2+}, Al^{3+}) and organic solvents (acetone, acetonitrile, ethanol, ethyl acetate, ethylene glycol, DCM, DMSO) was evaluated in detail. The influence of various metal ions on the activity of free and immobilized L-ASNase was investigated to evaluate the enzyme's stability in ion-rich environments (Fig. 5a). Co^{2+} and Mg^{2+} ions significantly enhanced the activity of both enzyme forms, which was in

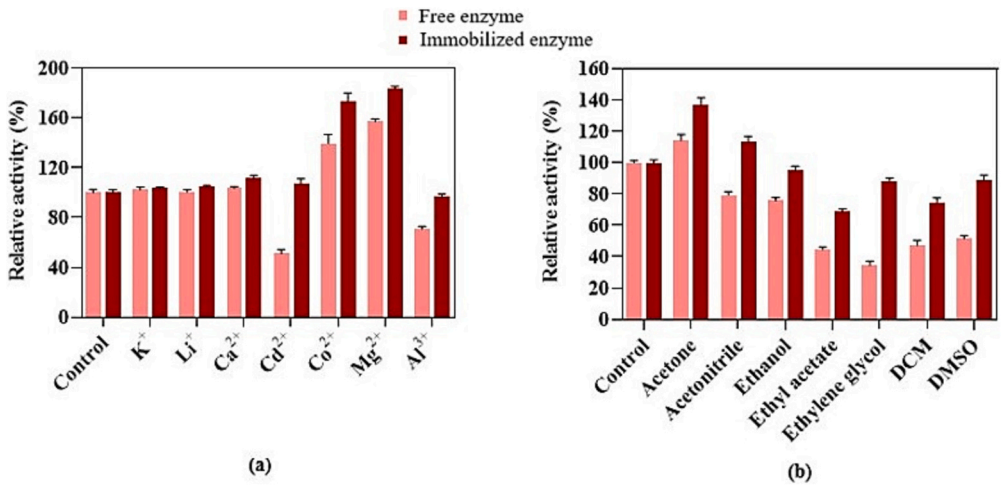

Fig. 5. Effect of (a) metal ions and (b) organic solvents on the free enzyme (L-ASNase) and immobilized enzyme (PHM-Cu^{2+}-L-ASNase) *Abbreviations*: L-ASNase, L-asparaginase; PHM—Cu^{2+}, poly(2-hydroxyethyl methacrylate–N-methacryloyl-(L)-histidine methyl ester–Cu^{2+}); DCM, dichloromethane; DMSO, dimethyl sulfoxide.

agreement with previous reports suggesting that these divalent cations acted as cofactors or structural stabilizers for L-ASNase [22]. In contrast, Cd^{2+} and Al^{3+} ions caused a marked reduction in the activity of the free enzyme—up to 30 % loss in the case of Al^{3+}—whereas the activity of the immobilized enzyme remained largely unaffected. This observation indicated that the PHM—Cu^{2+} immobilization matrix offered a degree of protection against metal ion-induced inhibition, likely by altering the enzyme's microenvironment and restricting access to surface residues. Such resistance was not observed in the free form, suggesting that immobilization imparted a shielding effect, particularly beneficial in metal-contaminated or complex industrial matrices. Additionally, K^{+}, Li^{+}, and Ca^{2+} ions had negligible impact on both enzyme forms, as reported in other studies as well [27]. The results demonstrated that the immobilized L-ASNase developed in this study was more robust against inhibitory metal ions, which may enhance its applicability in pharmaceutical and industrial settings where metal ion exposure was a common challenge.

The solvent stability of free and immobilized L-ASNase was evaluated by determining relative activity after incubation with various organic solvents (Fig. 5b). The stability of the enzymes was evaluated in the presence of different solvents to simulate potential industrial and pharmaceutical conditions where enzymes may be exposed to non-aqueous or partially aqueous environments. Organic solvents can affect enzyme structure, activity, and stability by disrupting hydrophobic interactions or altering the hydration shell. Assessing the enzyme's tolerance to such solvents provides insight into its robustness and applicability in non-conventional media, such as in drug formulations, biotransformations, or biocatalysis in organic synthesis. For L-ASNase, solvent stability was especially critical due to its clinical use in leukemia treatment and potential applications in food and biotechnology industries. Pharmaceutical formulations and storage conditions may involve solvent exposure, while industrial uses often require operation in complex media. Therefore, evaluating solvent tolerance enabled to predict the enzyme's performance, stability, and structural integrity in different applications. The results showed that acetone enhanced the activity of both enzyme forms, likely due to its ability to partially expose hydrophobic residues, thereby facilitating substrate access. Interestingly, acetonitrile caused a decrease in the activity of free L-ASNase but an increse in the activity of PHM-Cu^{2+}-L-ASNase, highlighting the stabilizing effect of immobilization against denaturing solvents. Moreover, ethanol, ethylene glycol, DCM, and DMSO significantly reduced the relative activity of the free enzyme (by 25–66 %), while they had negligible effects on the immobilized enzyme. These observations suggested that immobilization not only protected the enzyme's active conformation but also reduced its dependence on aqueous solvation, potentially by lowering flexibility or shielding water-sensitive domains. The results were in agreement with prior findings that enzymes with reduced hydration requirements exhibited higher stability and activity in organic media [32].

3.8. *In vitro* half-life

The *in vitro* half-life of free and immobilized L-ASNase was evaluated in artificial human serum medium to assess their biocompatibility and stability under physiologically relevant conditions (Fig. 6). Over a 7-day incubation period, a gradual decline in enzymatic activity was observed for both enzyme forms. However, the PHM-Cu^{2+}-L-ASNase demonstrated superior stability, retaining 56.87 % of its initial activity, while the free enzyme retained only 38.98 %. The result suggested that immobilization confered significant protection against enzymatic degradation or denaturation in serum-like environments. The improved stability may be attributed to the structural reinforcement provided by the immobilization matrix, which shields sensitive regions of the enzyme from proteolytic attack and conformational destabilization.

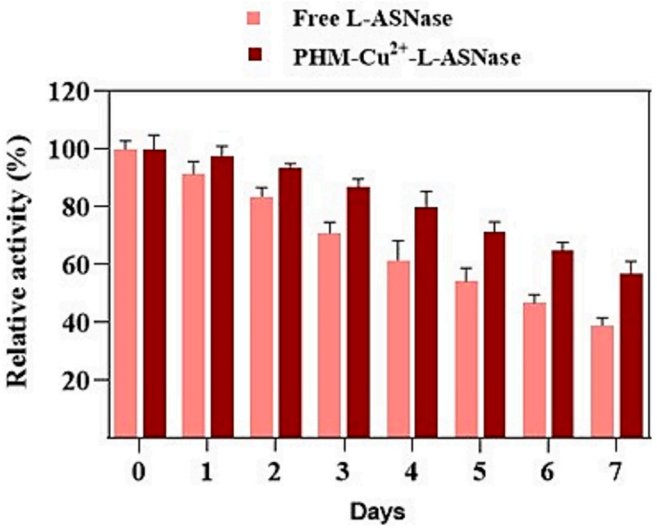

Fig. 6. *In vitro* half-life of the free enzyme (L-ASNase) and immobilized enzyme (PHM-Cu^{2+}-L-ASNase) *Abbreviations*: L-ASNase, L-asparaginase; PHM—Cu^{2+}, poly(2-hydroxyethyl methacrylate–N-methacryloyl-(L)-histidine methyl ester–Cu^{2+}).

Similar enhancements have been reported in the literature: Orhan and Uygun [26] found that immobilized L-ASNase retained 30 % of its activity after 40 days of storage, while the free enzyme lost all activity; Noma et al. [27] observed that cryogel-immobilized L-ASNase maintained 54 % activity after 28 days. Compared to these studies, the performance of PHM-Cu^{2+}-L-ASNase in artificial serum medium was both consistent and favorable, highlighting its potential utility for therapeutic applications where prolonged activity in biological fluids was essential.

The *in vitro* inactivation kinetics of free and PHM-Cu^{2}-L-ASNase in artificial human serum were also evaluated using first-order, Weibull distribution, and biphasic models. Key parameters, including rate constants (*k*), model-specific parameters, R^2, and half-life ($t_{1/2}$), are summarized in Table 4.

For the free enzyme, both the first-order (R^2adj = 0.9840) and Weibull distribution (R^2adj = 0.9979) models showed excellent fit, with comparable half-life values of approximately 5.5–5.7 days. The shape parameter n = 1.234 obtained from the Weibull distribution model indicated a slightly accelerating inactivation behavior. In contrast, the biphasic model yielded no significant improvement (R^2adj = 0.9776) and no clear phase separation ($k_1 \approx k_2$), suggesting that the inactivation proceeded as a single-phase process. For the immobilized enzyme, the Weibull distribution model provided the best fit (R^2adj = 0.9994), with a shape parameter $n = 1.614$ and a calculated half-life of 7.96 days, reflecting time-dependent acceleration. As with the free enzyme, the biphasic model did not improve fit quality (R^2adj = 0.9058) and produced nearly identical rate constants for both phases, indicating no meaningful kinetic separation. Consequently, the PHM—Cu^{2+} immobilization matrix significantly enhanced enzyme stability in artificial serum, extending the half-life by ~2 days.

3.9. L-ASNase binding analysis

The molecular interaction between L-ASNase and the PHM—Cu^{2+} nanoparticles was characterized in detail using SPR spectroscopy, which enabled real-time analysis of the binding process. The SPR sensorgrams revealed a concentration-dependent increase in resonance signal (ΔR%), confirming the specific binding of L-ASNase to the nanoparticle-modified surface. The binding capability of the L-ASNase in aqueous solutions was evaluated using various enzyme concentrations. The concentration of L-ASNase was systematically varied between 100 UI/mL and 2000 UI/mL. Fig. 7A illustrates the sensorgrams (ΔR%/time) for L-ASNase solutions at different concentrations. The SPR sensorgrams exhibited cycles of equilibrium, binding, dissociation, and re-equilibration. The observed increase in ΔR% with rising L-ASNase concentration indicated that the L-ASNase molecules were binding to the nanoparticles on the SPR sensor's surface, resulting in a measurable sensor response. As the binding sites became saturated, equilibrium was ultimately reached. As shown in Fig. 7B, the response of the SPR sensor demonstrated a linear increase with increasing L-ASNase concentration, showing a correlation coefficient of 0.97.

To quantitatively describe the binding interaction, several adsorption isotherm models were applied, including the Langmuir, Freundlich, Langmuir-Freundlich, and Scatchard models [73,74]. The model parameters were calculated from the sensorgram data using the following equations and given in Table 5.

$$Scatchard\ Equation\ \frac{\Delta R_{ex}}{[C]} = K_A\left(\Delta R_{max} - \Delta R_{eq}\right) \tag{8}$$

$$Langmuir\ Isotherm\ \Delta R = \left\{\frac{\Delta R_{max}[C]}{K_D} + [C]\right\} \tag{9}$$

$$Freundlich\ Isotherm\ \Delta R = DR_{max}[C]^{1/n} \tag{10}$$

$$Langmuir - Freundlich\ Isotherm\ \Delta R = \left\{\frac{\Delta R_{max}[C]^{1/n}}{K_D} + [C]^{1/n}\right\} \tag{11}$$

In the equations, ΔR represents the SPR signal measured after binding, and C represents the enzyme concentration. K_A and K_D are the binding and dissociation constants, respectively. 1/n is the exponent in the Freundlich equation.

Among the isotherm models applied, the Langmuir model exhibited the best fit (R^2 = 0.995), indicating monolayer adsorption on a homogeneously functionalized surface with a finite number of binding sites. K_D was calculated as 0.016 IU/mL, suggesting a strong binding affinity between the enzyme and the PHM—Cu^{2+} support matrix. The high affinity was particularly advantageous for enzyme immobilization, as it ensured firm yet reversible binding that maintained enzymatic activity without desorption or denaturation. The data also impled that the binding mechanism was likely governed by coordination interactions between functional groups on the enzyme surface and the Cu^{2+} ions within the polymer matrix, supporting the structural integrity of the immobilized enzyme. These findings were consistent with previous reports that emphasized the importance of stable, high-affinity binding in developing efficient and reusable immobilized enzyme systems. Thus, the SPR-based analysis provided strong molecular-level evidence that the PHM—Cu^{2+} nanoparticles were suitable carriers for L-ASNase immobilization, offering both high binding affinity and controlled interaction kinetics.

Table 4
Kinetic parameters for the inactivation of free enzyme (L-ASNase) and immobilized enzyme (PHM-Cu^{2+}-L-ASNase) in artificial human serum.

Enzyme	Model	k (day^{-1})	Parameter	R^2adj	$t_{1/2}$ (day)
L-ASNase	First-order	0.122		0.9840	5.68
	Biphasic	$k_1 = k_2$ = 0.122	f = 0.5084	0.9776	Fast: 5.64, slow: 5.72
	Weibull distribution	0.0849	n = 1.234	0.9979	5.48
PHM-Cu^{2+}-L-ASNase	First-order	0.066		0.9327	10.4
	Biphasic	$k_1 = k_2$ = 0.067	f = 0.2141	0.9058	Fast: 10.28, slow: 10.43
	Weibull distribution	k = 0.0243	n = 1.614	0.9994	7.96

Abbreviations: L-ASNase, L-asparaginase; PHM—Cu^{2+}, poly(2-hydroxyethyl methacrylate–N-methacryloyl-(L)-histidine methyl ester–Cu^{2+}); k, inactivation constant; $t_{1/2}$, half-life; R^2adj, adjusted coefficient of determination; f, fraction of rapidly inactivated enzyme; n, shape parameter.

4. Conclusion

This study presented the successful design, synthesis, and application of PHM—Cu^{2+} nanoparticles as efficient support matrices for L-ASNase immobilization. The coordination-based binding *via* Cu^{2+} ions enabled high immobilization efficiency while preserving enzymatic activity. The immobilized enzyme showed remarkable enhancements in thermal stability, storage durability, protease resistance, and reusability. The PHM-Cu^{2+}-L-ASNase exhibited enhanced thermal, storage, and *in vitro* serum stability compared to the free enzyme. Immobilization decreased the inactivation rate and extended the enzyme's half-life under all tested conditions, confirming the stabilizing effect of the PHM—Cu^{2+} matrix and its suitability for therapeutic enzyme applications. Kinetic studies confirmed the improved substrate affinity, and SPR analysis provided molecular-level evidence of high-affinity interactions governed by Langmuir-type adsorption. Furthermore, the immobilized enzyme demonstrated excellent performance in biologically relevant conditions, including artificial serum, metal ion-rich environments, and organic solvent systems. As a result, the PHM-Cu^{2+}-L-ASNase offered a balanced combination of structural integrity, catalytic efficiency, and long-term usability. The PHM—Cu^{2+} nanoparticles are not only effective carriers for enzyme immobilization but also contribute to the functional enhancement of L-ASNase. The PHM-Cu^{2+}-L-ASNase nanoparticles hold strong potential for integration into advanced drug delivery, biosensing,

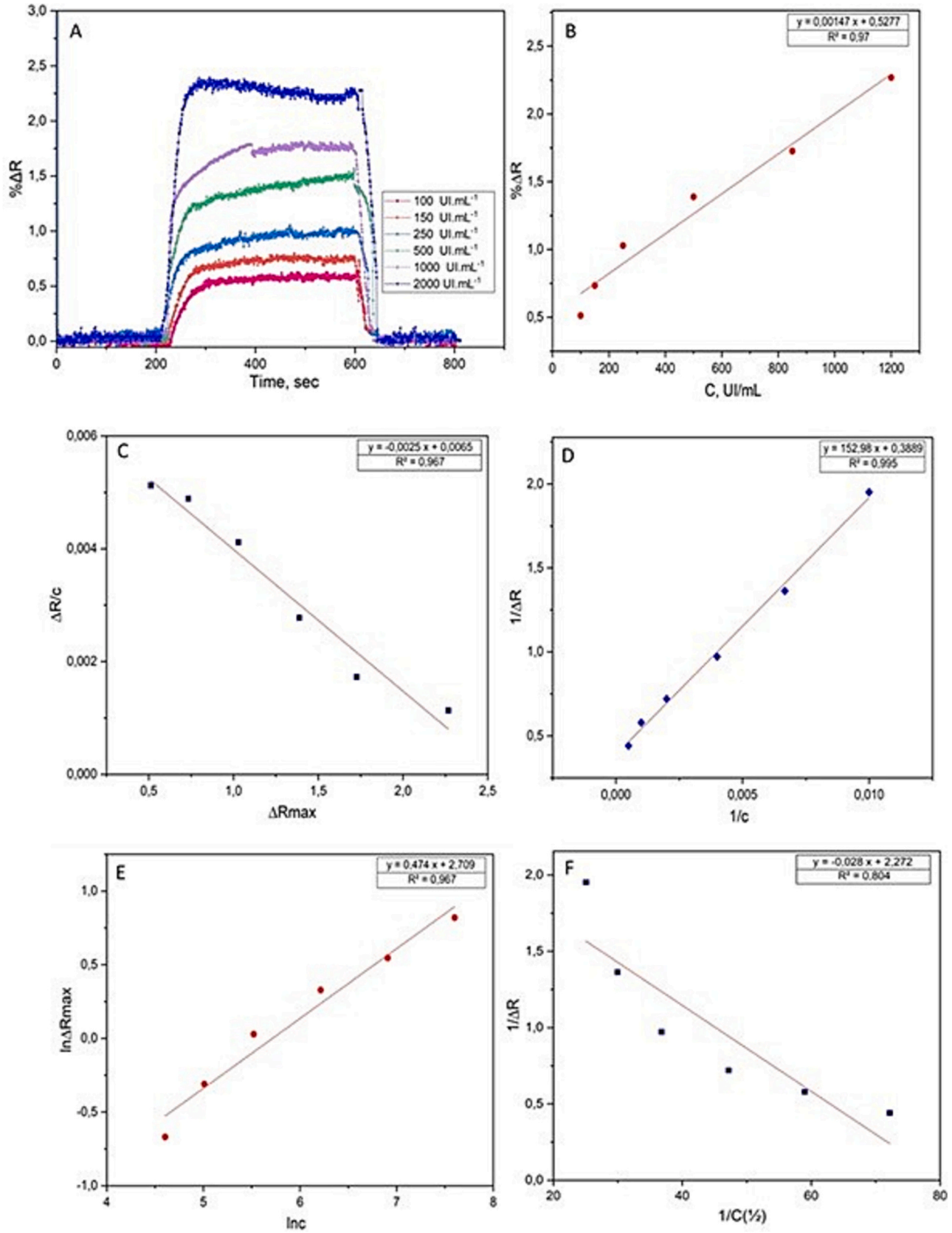

Fig. 7. (A) The real-time response of the SPR sensor for L-ASNase binding, concentration: 100–2000 IU/mL, flow rate: 150 μL/min, V: 10 mL, (B) the calibration graph for L-ASNase; Equilibrium binding analysis using the experimental calibration; (C) Scatchard method, (D) Langmuir, (E) Freundlich, (F) Langmuir-Freundlich isotherm models *Abbreviations*: SPR, surface plasmon resonance; L-ASNase, L-asparaginase; IU, international unit.

Table 5
Equilibrium binding analysis of L-ASNase on the modified SPR sensor surface, utilizing several isotherm models: Scatchard, Langmuir, Freundlich, and Langmuir-Freundlich.

Equilibrium analysis (Scatchard)		Langmuir		Freundlich		Langmuir-Freundlich	
ΔR_{max}	2.6	ΔR_{max}	2.57	ΔR	8.2	ΔR	0.44
K_A/(mL/IU)	0.0025	K_A/(mL/IU)	59.4	R^2	0.967	K_A/(mL/IU)	0.012
K_D (IU/mL)	400	K_D (IU/mL)	0.016			K_D (IU/mL)	81.07
R^2	0.967	R^2	0.995			R^2	0.804

Abbreviations: ΔRmax, maximum response change; K_A, association constant; K_D, dissociation constant; R^2, coefficient of determination.

and biocatalytic systems. Although the immobilized L-ASNase exhibited improved stability, substrate affinity, and reusability, certain limitations should be acknowledged. The turnover number (kcat) decreased after immobilization, which may slightly reduce catalytic efficiency under specific conditions. In addition, stability tests were conducted over limited time scales and in selected artificial serum conditions; therefore, long-term performance in complex biological media is still not fully determined. Further studies are needed to assess *in vivo* applicability.

CRediT authorship contribution statement

Kübra Kaya: Writing – original draft, Investigation, Formal analysis, Data curation. **Samir Abbas Ali Noma:** Writing – original draft, Methodology, Investigation, Formal analysis, Data curation. **Monireh Bakhshpour-Yücel:** Resources, Methodology, Investigation, Funding acquisition, Formal analysis. **Bilgen Osman:** Writing – review & editing, Supervision, Conceptualization.

Declaration of Generative AI and AI-assisted technologies in the writing process

During the preparation of this work the authors used CHATGPT in order to improve language and readability. After using this tool, the authors reviewed and edited the content as needed and take full responsibility for the content of the publication.

Declaration of competing interest

The authors declare that they have no known competing financial interests or personal relationships that could have appeared to influence the work reported in this paper.

Acknowledgments

This study was supported by Bursa Uludag University Research Foundation (Project no. FGA-2023-1538).

Appendix A. Supplementary data

Supplementary data to this article can be found online at https://doi.org/10.1016/j.ijbiomac.2025.147259.

Data availability

Data were given in the supporting information.

References

[1] C. Garcia-Galan, Á. Berenguer-Murcia, R. Fernandez-Lafuente, R.C. Rodrigues, Potential of different enzyme immobilization strategies to improve enzyme performance, Adv. Synth. Catal. 353 (2011) 2885–2904.
[2] E.F. Armstrong, Enzymes: a discovery and its consequences, Nature 131 (1933) 535–537.
[3] E.T. Özer, A.G. Sarıkaya, B. Osman, Adsorption and removal of diethyl phthalate from aqueous media with poly(hydroxyethyl methacrylate) nanobeads, Desalin. Water Treat. 57 (2016) 28864–28874.
[4] J.J.M. Cachumba, F.A.F. Antunes, G.F.D. Peres, L.P. Brumano, J.C. Santos, S.S. D. Silva, Current applications and different approaches for microbial L-asparaginase production, Braz. J. Microbiol. 47 (2016) 77–85.
[5] G. Shakambari, B. Ashokkumar, P. Varalakshmi, L-asparaginase – a promising biocatalyst for industrial and clinical applications, Biocatal. Agric. Biotechnol. 17 (2019) 213–224.
[6] A.H. Chheda, M.R. Vernekar, A natural preservative ε-poly-L-lysine: fermentative production and applications in food industry, Int. Food Res. J. 22 (2015) 23–28.
[7] S. Zuo, T. Zhang, B. Jiang, W. Mu, Reduction of acrylamide level through blanching with treatment by an extremely thermostable L-asparaginase during French fries processing, Extremophiles 19 (2015) 841–851.
[8] F. Pedreschi, K. Kaack, K. Granby, The effect of asparaginase on acrylamide formation in French fries, Food Chem. 109 (2008) 386–392.
[9] J.G. Dhanam, S. Kannan, L-asparaginase – types, perspectives and applications, Adv. Biotech. 13 (2013) 1–5.
[10] M. Pennisi, G. Malaguarnera, V. Puglisi, L. Vinciguerra, M. Vacante, M. Malaguarnera, Neurotoxicity of acrylamide in exposed workers, Int. J. Environ. Res. Public Health 10 (2013) 3843–3854.
[11] D.V. Zyzak, R.A. Sanders, M. Stojanovic, D.H. Tallmadge, B.L. Eberhart, D. K. Ewald, D.C. Gruber, T.R. Morsch, M.A. Strothers, G.P. Rizzi, M.D. Villagran, Acrylamide formation mechanism in heated foods, J. Agric. Food Chem. 51 (2003) 4782–4787.
[12] N.S.M. Kumar, C.A. Shimray, D. Indrani, H.K. Manonmani, Reduction of acrylamide formation in sweet bread with L-asparaginase treatment, Food Bioprocess Technol. 7 (2014) 741–748.
[13] A.C.V. Porto, O. Freitas-Silva, E.F. Souza, L.M.F. Gottschalk, Effect of asparaginase enzyme in the reduction of asparagine in green coffee, Beverages 5 (32) (2019).
[14] H.V. Hendriksen, B.A. Kornbrust, P.R. Østergaard, M.A. Stringer, Evaluating the potential for enzymatic acrylamide mitigation in a range of food products using an asparaginase from Aspergillus oryzae, J. Agric. Food Chem. 57 (2009) 4168–4176.
[15] F. Morales, E. Capuano, V. Fogliano, Mitigation strategies to reduce acrylamide formation in fried potato products, Ann. N. Y. Acad. Sci. 1126 (2008) 89–100.
[16] N. Verma, M. Bansal, S. Kumar, Whole cell based miniaturized fiber optic biosensor to monitor L-asparagine, Adv. Appl. Sci. Res. 3 (2012) 809–814.
[17] D. Castro, A.S.C. Marques, M.R. Almeida, G.B. de Paiva, H.B. Bento, D.B. Pedrolli, V.C. Santos-Ebinuma, L-asparaginase production review: bioprocess design and biochemical characteristics, Appl. Microbiol. Biotechnol. 105 (2021) 4515–4534.
[18] S.A. Mohamed, M.F. Elshal, T.A. Kumosani, A.M. Aldahlawi, Purification and characterization of asparaginase from Phaseolus vulgaris seeds, Evid. Based Complement. Alternat. Med. 2015 (2015) 456701.
[19] A. Vina, P. Semjonovs, P. Zikmanis, Levan as a support for enzyme immobilization, J. Biotechnol. 91 (2001) 151–158.
[20] K. Ghosh, U.S. Ghosh, P.K. Ghosh, Immobilization of L-asparaginase on polyaniline nanofibers, Process Biochem. 47 (2012) 1394–1401.
[21] A. Ulu, B. Ates, D. Atila, Biodegradable pHEMA–starch composite as a support for enzyme immobilization, Bioprocess Biosyst. Eng. 38 (2015) 1857–1864.
[22] A. Ulu, D. Atila, B. Ates, Immobilization of L-asparaginase onto P(MAA-co-MMA)-starch composites, Int. J. Biol. Macromol. 91 (2016) 250–259.
[23] M.S. Bahraman, I. Alemzadeh, Optimization of L-asparaginase immobilization using RSM, Biochem. Eng. J. 119 (2017) 42–49.
[24] M. Monajati, M. Azizi, H. Zare, Graphene oxide functionalization and enzyme immobilization, Enzym. Microb. Technol. 115 (2018) 52–59.
[25] A.A. Haroun, M. Elshikh, S.S. Al-Deyab, Immobilization of L-asparaginase from fungi on ox-MWCNTs, J. Mol. Catal. B Enzym. 173 (2020) 65–73.
[26] H. Orhan, D.A. Uygun, Magnetic poly(HEMA-GMA) nanoparticles for L-asparaginase immobilization, Int. J. Biol. Macromol. 153 (2020) 751–759.
[27] S.A. Noma, N.M. Hashim, S.S. Mahmod, Functionalized Fe_3O_4/SiO_2 nanoparticles for enzyme immobilization, Mater. Sci. Eng. C Mater. Biol. Appl. 109 (2020) 110556.
[28] S.A. Noma, N.M. Hashim, S.S. Mahmod, Cryogel-based immobilization of L-asparaginase, Int. J. Biol. Macromol. 170 (2021) 251–259.
[29] T. Tarhan, S. Balcıoğlu, E. Akyüz, Immobilization of L-asparaginase on polymeric Fe_3O_4@Au-CMC nanoparticles, Biotechnol. Appl. Biochem. 69 (2022) 944–953.
[30] C.H.N. Barros, D.P. Queiroz, V.M. Cardoso, Carbon xerogels as supports for enzyme immobilization, Int. J. Biol. Macromol. 195 (2022) 213–222.
[31] M. Iraninasab, M. Salehi, M. Mohammadi, PAMAM-G3@ZnO-Cs nanocarriers for L-asparaginase delivery, Carbohydr. Polym. 308 (2023) 120582.
[32] Ö. Acet, Smart nanopolymers for pH and temperature-responsive enzyme delivery, Int. J. Biol. Macromol. 229 (2023) 420–430.
[33] E. Bahreini, K. Aghaiypour, R. Abbasalipourkabir, A.R. Mokarram, M.T. Goodarzi, M. Saidijam, Preparation and nanoencapsulation of L-asparaginase II in chitosan-tripolyphosphate nanoparticles and in vitro release study, Nanoscale Res. Lett. 9 (2014) 340.
[34] A. Ulu, S. Koytepe, B. Ates, Design of starch functionalized biodegradable P(MAA-co-MMA) as carrier matrix for L-asparaginase immobilization, Carbohydr. Polym. 153 (2016) 559–572.
[35] A. Ulu, S. Koytepe, B. Ates, Synthesis and characterization of biodegradable pHEMA-starch composites for immobilization of L-asparaginase, Polym. Bull. 73 (2016) 1891–1907.

[36] M. Bakhshpour, A.K. Piskin, H. Yavuz, A. Denizli, Quartz crystal microbalance biosensor for label-free MDA-MB-231 cancer cell detection via notch-4 receptor, Talanta 204 (2019) 840–845.
[37] M. Bakhshpour, A. Derazshamshir, N. Bereli, A. Elkak, A. Denizli, [PHEMA/PEI]–Cu(II) based immobilized metal affinity chromatography cryogels: application on the separation of IgG from human plasma, Mater. Sci. Eng. C 61 (2016) 824–831.
[38] M. Jalilzadeh, L. Uzun, S. Şenel, A. Denizli, Specific heavy metal ion recovery with ion-imprinted cryogels, J. Appl. Polym. Sci. 133 (2016) 10.
[39] H. Shaikh, G. Sener, N. Memon, M.I. Bhanger, S.M. Nizamani, R. Üzek, A. Denizli, Molecularly imprinted surface plasmon resonance (SPR) based sensing of bisphenol A for its selective detection in aqueous systems, Anal. Methods 7 (2015) 4661–4670.
[40] M. Bakhshpour, H. Yavuz, A. Denizli, Controlled release of mitomycin C from PHEMAH–Cu(II) cryogel membranes, Artif. Cells Nanomed. Biotechnol. 46 (2018) 946–954.
[41] L.T. Mashburn, Tumor inhibitory effect of L-asparaginase from Escherichia coli, Arch. Biochem. Biophys. 105 (1964) 450–452.
[42] B. Osman, A. Kara, N. Beşirli, Immobilization of glucoamylase onto Lewis metal ion chelated magnetic affinity sorbent: kinetic, isotherm and thermodynamic studies, J. Macromol. Sci. A 48 (2011) 387–399.
[43] A. Kara, B. Osman, H. Yavuz, N. Beşirli, A. Denizli, Immobilization of α-amylase on Cu^{2+} chelated poly(ethylene glycol dimethacrylate-n-vinyl imidazole) matrix via adsorption, React. Funct. Polym. 62 (2005) 61–68.
[44] B. Osman, A. Kara, L. Uzun, N. Beşirli, A. Denizli, Vinyl imidazole carrying metal-chelated beads for reversible use in yeast invertase adsorption, J. Mol. Catal. B Enzym. 37 (2005) 88–94.
[45] B. Osman, A. Kara, E. Demirbel, N. Beşirli, A. Denizli, Adsorption equilibrium, kinetics and thermodynamics of α-amylase on poly(DVB-VIM)–Cu^{2+} magnetic metal-chelate affinity sorbent, Appl. Biochem. Biotechnol. 168 (2012) 279–294.
[46] S. Kök, B. Osman, A. Kara, N. Beşirli, Vinyl triazole carrying metal-chelated beads for the reversible immobilization of glucoamylase, J. Appl. Polym. Sci. 120 (2011) 2563–2570.
[47] T. Çam, B. Osman, A. Kara, E. Demirbel, N. Beşirli, G. Irez, Potentiometric, kinetic, and thermodynamic investigations into Cu^{2+} ion binding properties of vinyl imidazole containing IMAC adsorbent, J. Appl. Polym. Sci. 131 (2014) 39751.
[48] R.C.F. Cheung, J.H. Wong, T.B. Ng, Immobilized metal ion affinity chromatography: a review on its applications, Appl. Microbiol. Biotechnol. 96 (2012) 1411–1420.
[49] T. Yabutani, H. Sumi, T. Nakamura, S. Akatsuki, T.X. Le, Multielemental elution behavior of metal ions adsorbed on iminodiacetic acid chelating resin by using hydrogen peroxide as an eluent, Anal. Sci. 28 (2012) 463–468.
[50] S.T. Loughran, D. Walls, Purification of poly-histidine-tagged proteins, in: D. Walls, T.S. Loughran (Eds.), Protein Chromatography: Methods and Protocols, Humana Press, New York, 2011, pp. 311–335.
[51] W.H.K. Kuo, H.A. Chase, Exploiting the interactions between poly-histidine fusion tags and immobilized metal ions, Biotechnol. Lett. 33 (2011) 1075–1084.
[52] M. Bakhshpour, A.K. Piskin, H. Yavuz, A. Denizli, Quartz crystal microbalance biosensor for label-free MDA-MB-231 cancer cell detection via notch-4 receptor, Talanta 204 (2019) 840–845.
[53] I. Göktürk, M. Bakhshpour, D. Çimen, F. Yılmaz, N. Bereli, A. Denizli, SPR signal enhancement with silver nanoparticle-assisted plasmonic sensor for selective adenosine detection, IEEE Sensors J. 22 (2022) 14862–14869.
[54] S.D. Gür, M. Bakhshpour, A. Denizli, Nanoscale SPR sensor for the ultrasensitive detection of the ovarian cancer marker carbohydrate antigen 125, New J. Chem. 46 (2022) 7263–7270.
[55] R. Chouhan, A.K. Bajpai, Real time in vitro studies of doxorubicin release from PHEMA nanoparticles, J. Nanobiotechnol. 7 (2009) 12.
[56] S.M. Paterson, A.M. Shadforth, D.H. Brown, P.W. Madden, T.V. Chirila, M.V. Baker, The synthesis and degradation of collagenase-degradable poly(2-hydroxyethyl methacrylate)-based hydrogels and sponges for potential applications as scaffolds in tissue engineering, Mater. Sci. Eng. C 32 (2012) 2536–2544.
[57] N. Oh, J.H. Park, Endocytosis and exocytosis of nanoparticles in mammalian cells, Int. J. Nanomedicine 9 (2014) 51–63.
[58] A. Albanese, P.S. Tang, W.C.W. Chan, The effect of nanoparticle size, shape, and surface chemistry on biological systems, Annu. Rev. Biomed. Eng. 14 (2012) 1–16.
[59] O. Cakir, A molecularly imprinted nanofilm-based quartz crystal microbalance sensor for the real-time detection of pirimicarb, J. Mol. Recognit. 32 (2019) e2785.
[60] J.D. Clogston, A.K. Patri, Zeta potential measurement, in: Characterization of Nanoparticles Intended for Drug Delivery, Humana Press, 2011, pp. 63–70.
[61] L. Qi, Z. Xu, X. Jiang, C. Hu, X. Zou, Preparation and antibacterial activity of chitosan nanoparticles, Carbohydr. Res. 339 (2004) 2693–2700.
[62] A.M. Mittelman, J.D. Fortner, K.D. Pennell, Effects of ultraviolet light on silver nanoparticle mobility and dissolution, Environ. Sci. Nano 2 (2015) 683–691.
[63] V. Domínguez-Villegas, B. Clares-Naveros, M.L. García-López, A.C. Calpena-Campmany, P. Bustos-Zagal, M.L. Garduño-Ramírez, Development and characterization of two nano-structured systems for topical application of flavanones isolated from Eysenhardtia platycarpa, Colloids Surf. B: Biointerfaces 116 (2014) 183–192.
[64] T. Suponik, M. Lemanowicz, P. Wrona, Stability of green tea nanoscale zero-valent iron, E3S Web Conf. 8 (2016) 01048.
[65] A. Baluchi, A. Homaei, Immobilization of L-asparaginase on chitosan nanoparticles for the purpose of long-term application, Int. J. Biol. Macromol. 257 (2024) 128655.
[66] N. Ortega, S. de Diego, J.M. Rodríguez-Nogales, M. Perez-Mateos, M.D. Busto, Kinetic behaviour and thermal inactivation of pectinlyase used in food processing, Int. J. Food Sci. Technol. 39 (2004) 631–639.
[67] C.A. Weemaes, L.R. Ludikhuyze, I. van den Broeck, M. Hendrickx, Kinetics of combined pressure–temperature inactivation of avocado polyphenol oxidase, Biotechnol. Bioeng. 60 (1998) 292–300.
[68] C.S. Chen, M.C. Wu, Kinetic models for thermal inactivation of multiple pectinesterases in citrus juice, J. Food Sci. 63 (1998) 747–750.
[69] M.G. Corradini, M. Peleg, A model of non-isothermal degradation of nutrients, pigments and enzymes, J. Sci. Food Agric. 84 (2004) 217–226.
[70] F.M. Veronese, A. Mero, The impact of PEGylation on biological therapies, BioDrugs 22 (2008) 315–329.
[71] A. Radadiya, W. Zhu, A. Coricello, S. Alcaro, N.G.J. Richards, Improving the treatment of acute lymphoblastic leukemia, Biochemistry 59 (2020) 3193–3200.
[72] H.J. Müller, A. Höhne, L-asparaginase treatment in acute lymphoblastic leukemia: a focus on PEGylated formulations, Cancer Chemother. Pharmacol. 73 (2014) 951–962.
[73] B. Osman, L. Uzun, N. Beşirli, A. Denizli, Microcontact imprinted surface plasmon resonance sensor for myoglobin detection, Mater. Sci. Eng. C 33 (2013) 3609–3614.
[74] A. Göçenoğlu Sarıkaya, B. Osman, T. Çam, A. Denizli, Molecularly imprinted surface plasmon resonance (SPR) sensor for uric acid determination, Sensors Actuators B Chem. 251 (2017) 763–772.